Journal of Power Sources 214 (2012) 358–364

Contents lists available at SciVerse ScienceDirect

Journal of Power Sources

journal homepage: www.elsevier.com/locate/jpowsour

A single step solution combustion approach for preparing gadolinia doped ceria solid oxide fuel cell electrolyte material suitable for wet powder and plasma spraying processes

B. Shri Prakash, V.K. William Grips, S.T. Aruna*

Surface Engineering Division, Council of Scientific and Industrial Research-National Aerospace Laboratories, Bangalore 560 017, Karnataka, India

HIGHLIGHTS

- Synthesis of wet powder sprayable $Gd_{0.2}Ce_{0.8}O_2-\delta$ powders by solution combustion.
- Synthesis of plasma sprayable $Gd_{0.2}Ce_{0.8}O_2-\delta$ powders by solution combustion.
- High sinteractivity and conductivity in nano sized $Gd_{0.2}Ce_{0.8}O_2-\delta$ powders.
- Fabrication of dense $Gd_{0.2}Ce_{0.8}O_2-\delta$ coating by atmospheric plasma spraying.

ARTICLE INFO

Article history:
Received 16 February 2012
Received in revised form
9 April 2012
Accepted 10 April 2012
Available online 28 April 2012

Keywords:
Solid oxide fuel cell
Electrolyte
Conductivity
Impedance spectroscopy

ABSTRACT

The present study explores the versatility of solution combustion method for preparing powders of varying characteristics suitable for intermediate temperature solid oxide fuel cell (IT-SOFC) fabrication. The promising electrolyte material for IT-SOFC, $Gd_{0.2}Ce_{0.8}O_{2-\delta}$ (GDC), is considered for the present investigation. GDC powders consisting of sub-micron sized particles (<250 nm) and micron sized (>20 μm) particles are produced by varying the fuel used in the combustion reaction. Highly sinteractive nano-GDC powders prepared using oxalyl dihydrazide as a fuel results in dense pellets with high conductivity (3×10^{-4} Scm^{-1} at 400 °C). This powder also results in a stable suspension suitable for wet powder spraying and electrophoretic deposition. Powders with larger particle size (>20 μm) prepared by solution combustion method using mixture of fuels, exhibits necessary flowability for atmospheric plasma spraying (APS). GDC coatings fabricated by APS using flowable powders are dense with superior adhesion between the splats. Good adhesion between the splats in the APS coatings is attributed to the higher level of melting of the combustion synthesized particles in the plasma flame owing to their low specific mass.

1. Introduction

In recent times the research and development on intermediate temperature solid oxide fuel cells (IT-SOFC) with an operating temperature of 400–700 °C has emerged as one of the active areas of investigations. IT-SOFCs provide a greater flexibility in the fabrication of electrodes, cell interconnectors and results in reduced thermal degradation and thermal cycling stresses [1–5]. Lowering of the operating temperature of SOFC however necessitates considerable reduction in the thickness (to few nm) of the conventionally used electrolytes such as yttria stabilized zirconia (YSZ) to minimize the ohmic losses. Though thin film electrolytes could well be fabricated by techniques such as chemical vapor deposition, physical vapor deposition, etc., these techniques are expensive both in terms of equipment and operation and are not most appropriate for commercialization [6]. Fortunately, availability of materials such as gadolinia doped ceria (GDC) with good ionic conductivity in the intermediate temperature range ($2–3 \times 10^{-2}$ Scm^{-1} at 650 °C) opens up an opportunity to use thick film electrolytes with low ohmic losses [7].

The present work is intended to explore the possibility of fabricating thick film of GDC electrolyte through fabrication methods that lead to the minimization of overall fabrication costs of SOFC. To achieve such a goal, wet powder spraying (WPS) and atmospheric plasma spraying (APS) are the potential methods. In

* Corresponding author. Tel.: +91 080 25086250; fax: +91 080 25210113.
E-mail address: aruna_reddy@nal.res.in (S.T. Aruna).

0378-7753/$ – see front matter © 2012 Elsevier B.V. All rights reserved.
doi:10.1016/j.jpowsour.2012.04.049

WPS, to achieve dense electrolyte coatings, it is generally required to sinter ceria based electrolytes at high temperature (~1400 °C). Ability to sinter the electrolyte layer at much lower temperature (~1250 °C and below) provides not only an opportunity to fabricate all the components of SOFC at the same temperature but also leads to the reduction in the fabrication costs. To obtain dense coatings at lower sintering temperatures, it is essential to synthesize sinteractive ultrafine powders. A wide variety of processes belonging to wet chemical routes are generally used for the synthesis of fine powders of ceria and doped ceria [5,8–13]. Simple and cost effective solution combustion synthesis (SCS) method could well be a potential option for the synthesis of electrolytic powder, if sinteractive nano-agglomerated powders can be prepared. Though SCS results in nano primary crystallites (often smaller than 10 nm), agglomerated particles are common due to the high reaction temperatures [14–16]. Agglomerates in the solution combustion synthesized powders retard the densification kinetics [17,18]. Weakly-agglomerated powder is essential not only for conventional dry processing methods (e.g. powder compaction), but also in other fabrication methods such as electrophoretic deposition, tape casting and wet powder spraying etc., to achieve stable suspensions [19]. The benefits expected from nanocrystallites are easily lost during the fabrication of components if weakly-agglomerated powders cannot be synthesized. The powder characteristics like crystallite size, surface area, extent and nature (hard or soft) of agglomeration of the powder produced by SCS are primarily governed by the enthalpy or flame temperature generated during combustion, rate of combustion and gases evolved during the reaction, which itself is dependent on the nature of the fuel and oxidizer to fuel (O/F) ratio. Hence in SCS, the fuel and O/F ratio need to be carefully chosen to achieve poorly agglomerated nanosized particles.

There is a scope for SOFC fabrication cost reduction by employing APS for electrolyte deposition and other components of SOFC, due to its advantages such as easy operation, easy automation, high deposition efficiency, single step fabrication, etc [20–24]. However, to obtain dense electrolyte coatings by APS, stock powder consisting of micron sized agglomerates (20–200 μm) with high flowability are necessary. Stock powders for APS are generally synthesized by different routes often involving multiple processing steps. Most of the methods reported in the literature employ an additional agglomeration step like spray drying to get plasma sprayable powders which makes these processes more expensive and laborious.

The main objective of the present work is to explore the versatility and novelty of solution combustion method in the preparation of GDC powders with particle sizes ranging from nano to micron size that are suitable for WPS and APS by using different fuels and mixture of fuels respectively. Attempt has also been made to establish the correlation between characteristics of the powders prepared using different fuels with their sinterability and eventually on its electrical conductivity. Powders with large agglomerate sizes and good flowability were tested for its suitability in APS.

2. Experimental

Gadolinia doped ceria ($Gd_{0.2}Ce_{0.8}O_{2-\delta}$) was prepared using solution combustion method by using the following starting raw materials: ceric ammonium nitrate, gadolinium oxide, glycine, oxalyl dihydrazide (ODH) and hexamethylenetetramine (HMT) and ammonium acetate (AA). The required molar ratio of gadolinium oxide, ceric ammonium nitrate and fuels was calculated based on the propellant chemistry, i.e. the ratio of oxidizer to fuel ratio should be unity ($O/F = 1$). Gadolinium oxide was first dissolved in dilute nitric acid to get gadolinium nitrate solution; to this solution aqueous ceric ammonium nitrate solution was added and stirred well. Stoichiometric amounts of fuels glycine/ODH/HMT/Glycine + ammonium acetate were added to the metal nitrate solution, stirred well and transferred into an alumina crucible. The alumina crucible was placed in a muffle furnace and the temperature was raised to 450 °C. The solution boils, froths and catches fire leading to a combustion reaction. Heat and gases were liberated during this reaction and an intense, self-sustained flame was formed. As-prepared powder from solution combustion process was pale yellow in color. As-synthesized GDC powders prepared using glycine, HMT, ODH and glycine + ammonium acetate fuels will be henceforth termed as GDC–glycine, GDC–HMT,GDC–ODH, GDC–glycine + AA, respectively.

Room temperature X-ray diffraction (XRD) studies of as-synthesized GDC powders were performed using Philips X'Pert PRO X-ray diffractometer. The average crystallite size of the powders was calculated from Scherrer's formula. Instrumental peak broadening was accounted for while calculating crystallite size. Particle size distribution of powders was analyzed using laser light scattering method (Mastersizer 2000, Malvern Instruments). For particle size analysis, as-calcined powders were well dispersed in 0.5 wt.% Calgon solution. Flowability of the powders was measured using a Hall flow meter according to ASTM B213-9. The morphology of the powders were examined using field emission scanning electron microscope (FESEM)(Carl Zeiss).

Circular pellets (~10 mm diameter) were prepared by uniaxial dry pressing at 200 MPa by using PVA as binder. The green pellets were sintered at 1300 °C/5 h. In addition to the conventional sintering, GDC–ODH samples were subjected to microwave sintering and two-stage sintering. Density measurements of GDC ceramic discs were carried out by using Archimedes principle. Sintered pellets were finely polished using 0.3 μm sized alumina and were thermally etched. Microstructure of the thermally etched samples and the level of porosity in the samples were examined by SEM studies on the surface and cross sectional surfaces of the sintered GDC disc samples.

For conductivity measurements, silver paste was applied on the flat parallel surfaces of the disc (cured at 1053 K) and Pt wires were connected. Two probe complex impedance measurements were carried out in the 473–873 K temperature range using Autolab potentiostat/galvanostat equipment. The analysis was performed in the frequency range of 0.1 Hz–1 MHz at signal strength of 10 mV.

Plasma spraying of the powders was performed by atmospheric air plasma spraying system (Sulzer Metco-9M) on aluminum rod (12 mm dia × 8 mm thickness). Plasma spray parameters used for spraying GDC powder are listed in Table 1. The surface and the cross sectional microstructure of the coating was examined by FESEM.

3. Result and discussion

Fig. 1 shows the XRD patterns of as-synthesized powders from solution combustion method using different fuels. The diffraction peaks from all the samples were indexed to a fluorite-type

Table 1
Plasma spray parameters used for spraying GDC powder.

Parameters for plasma spraying	Value
Argon Flow (NLPM)	42
Hydrogen Flow (NLPM)	13
Amps/Volts	550/55
Carrier gas Flow (bar)	4
Pre Heat/Spray passes	2/8
Powder Feed rate (g/min)	20
Gun speed (mm/min)	800
Spray distance (cm)	15
Substrate temperature (K)	873

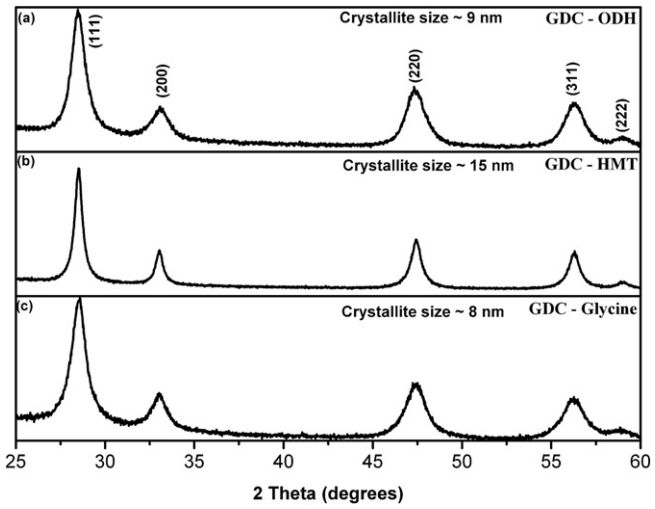

Fig. 1. XRD patterns of as-synthesized GDC powders prepared by solution combustion method using different fuels.

structure with cubic lattice symmetry (JCPDS card no. 4-0593). There were no traces of Gd_2O_3 peaks indicating the formation of solid solution. The broad peaks in the XRD pattern indicate the presence of nano-crystallites in all the samples. Elimination of calcination step was probably helpful in preventing the possible crystallite growth. Though peak widths are relatively wider in all the patterns, the level of peak broadening, which is a measure of the crystallite size, is different in different samples. Crystallite sizes calculated using Sherrer's formula are presented in Table 2. It can be noted that crystallite size is least in the case of GDC powders prepared from glycine fuel (~8 nm) and highest for the one's prepared using HMT (~15 nm). GDC from ODH had the intermediate crystallite size values (~9 nm). The varied intensity of yellow color observed in different GDC powders could be attributed to the varying crystallite sizes. Table 2 also depicts the particle size distribution of the powder. The average agglomerated particle sizes show that the combustion synthesized GDC powders are agglomerated due to the clustering of nano-crystallites (~10 nm as observed by line broadening). The combustion synthesized nano-crystallites agglomerate easily due to the strong Van der Waals forces between ultrafine crystallites. In the present case, although the average crystallite size was found to be in the range of ~10 nm in all the samples, there was a significant variation in the agglomerate size depending on the fuel used for the combustion reaction. From the particle size distribution data it is very much evident that the powders derived from glycine exhibits highest particle agglomeration (up to 85 μm) and those prepared by ODH exhibit least (up to 1 μm). Ratio between the particle size and the crystallite size, which provides the information on the extent of agglomeration in the powder, suggests that the ratio is highest for the powder derived from the glycine, though crystallite size is least in them (Table 2). Since the powders prepared using glycine and the ODH exhibit most contrasting characteristics, they were considered for more detailed study.

Table 2
Particle size, crystallite size and particle to crystallite ratio in the GDC powders prepared by SCS using different fuels.

Powder	Particle Size Analysis			Crystallite size (nm)	Particle/crystallite ratio d (0.5)/crystallite size
	d(0.1)	d(0.5)	d(0.9)		
GDC–glycine	9.944	21.516	40.280	~8	2689.5
GDC–HMT	0.968	3.192	31.987	~15	2132
GDC–ODH	0.094	0.280	1.107	~9	31

Fig. 2 shows the FESEM images of the as-prepared GDC powders synthesized from different fuels. In the case of GDC–ODH powders (Fig. 2a), particle sizes obtained from SEM and particle sizes analyses closely match (~200 nm). It can also be noted that these aggregates are very dense. On the contrary, as-prepared GDC–glycine powder consists of porous and loosely bound particles in the size range of 20 μm (Fig. 2b). However, upon thorough grinding, these agglomerates break in to finer and denser aggregates (~1 μm) (Fig. 2c). Bigger particles (15–20 μm) in the as-prepared GDC–glycine powder are likely formed due to the physical agglomeration of the smaller sized (~1 μm) fractal aggregates. With the reduced amount of glycine, % of agglomerated particles of GDC (XRD is not shown) increased. However, these agglomerates are softer in nature and are not suitable for plasma spraying due to the smaller size and low specific mass. The size and strength of the GDC agglomerates increased on using ammonium acetate along with glycine fuel and the resultant powder (GDC–glycine + AA) consisted of blocky angular shaped particles (Fig. 2d) (XRD not shown). Owing to the shape and size of the particles, GDC–glycine + AA powders exhibited the necessary flowability (100 s/50 g), for plasma spraying. However, the flowability was lower than the commercially plasma sprayable powders. Other GDC powders did not exhibit necessary flowability due to the small sized particles.

In the combustion reaction, the factors that influence the phase formation and powder characteristics (crystallite size, particle size, strength of agglomeration) are enthalpy of the reaction (heat evolved during the reaction), rate of the reaction (vigor of the reaction), gas evolved during the reaction, etc. These factors are in turn influenced by the nature of fuel and the oxidizer-to-fuel ratio used. Adiabatic temperature generated during the combustion reaction can be theoretically calculated or experimentally measured. Enthalpy of the reaction could also be determined by differential thermal analysis studies. However, above studies were not performed in the present study as the facilities were not available. Assuming complete combustion, the formation of GDC by two different fuels may be represented by the following equations.

$$0.2Gd(NO_3)_3\cdot 6H_2O + 0.8(NH_4)_2Ce(NO_3)_6 + C_2H_6N_4O_2(ODH) \xrightarrow{450^oC/Air} Ce_{0.8}Gd_{0.2}O_{1.9} + 5.5N_2 + 7.4H_2O + 2CO_2 + 3O_2$$

$$0.2Gd(NO_3)_3\cdot 6H_2O + 0.8(NH_4)_2Ce(NO_3)_6 + C_2H_5NO_2(glycine) \xrightarrow{450^{\circ}C/Air} Ce_{0.8}Gd_{0.2}O_{1.9} + 4N_2 + 6.9H_2O + 2CO_2 + 3.3O_2$$

Though the gases evolved during the combustion reaction by using glycine (16 mol) and ODH (18 mol) are nearly identical, vast differences were observed in the powder characteristics. This may be due to the differences in the heat evolved during the two reactions. Literature survey reveals that heat evolved with glycine as a fuel is generally higher and the visual observation of the intensity of the combustion flame under study corroborated the same. On the other hand, the main feature of ODH fuel is that (i) it is hydrazine based and therefore contains a potent N–N bond and (ii) they are water soluble and combustible with low ignition temperature. It can thus be concluded that porous agglomerates (aggregates of nano-crystallites) in GDC–glycine powders is due to the cumulative effect of these factors. In comparison to GDC–glycine reaction, combustion reaction involving ODH as a fuel was less flaming and sluggish. The lower level of agglomeration of GDC–ODH powders may be attributed to the evolution of large number of gases.

Fig. 3 shows the SEM images of the sintered (1300 °C/5 h), polished and thermally etched surface of GDC samples prepared

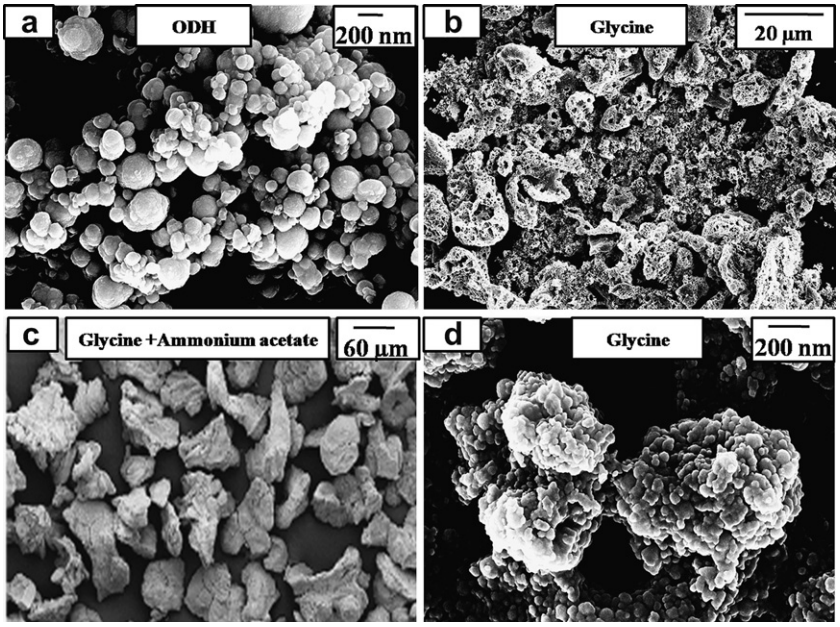

Fig. 2. FESEM images of as-prepared GDC powders synthesized using different fuels.

from GDC powders synthesized using glycine, HMT, and ODH fuels. It is evident from the microstructure that GDC–glycine and GDC–HMT powders have resulted in a porous microstructure (Fig. 3a and b) though sub-micron sized crystallites within the agglomerates of the original powder are retained. It can be inferred from these microstructures that GDC–HMT and GDC–glycine powders are not suitable for the electrolyte layer deposition as they lead to well connected pores in the sintered pellets. Highly porous microstructure obtained in the case of GDC–glycine + AA (not shown in the figure) is not surprising as powder characteristics of GDC–glycine + AA and GDC–glycine are nearly similar. On the other hand, powders from GDC–ODH resulted in a well sintered, dense, pore free microstructure with a grain size in the range of 2–3 μm (Fig. 3c). Superior sinteractivity of GDC–ODH powders can be attributed to the presence of small and dense aggregates. These observations signify the importance of characteristics of the starting powders in controlling the final microstructure. If achieving a dense coating at low temperature is important from the fabrication view point, concurrent retention of small grains is doubly advantageous as it would have positive bearing on the mechanical properties of the coatings. In addition, many researchers have observed an increased ionic conductivity with decrease in grain size, especially when the size is below ~100 nm. Increased conduction in these samples has been attributed to the dominance of interface-controlled ion migration. Some reports have claimed increased conductivity even in the higher grain size range (300–400 nm). In the present investigation, densification strategies were modified with the intention of attaining these twin objectives. Densification engineering is of great significance, especially in nano-materials such as GDC–ODH, as nano-ceramics grow and sinter in a pretty different way than larger scaled powders.

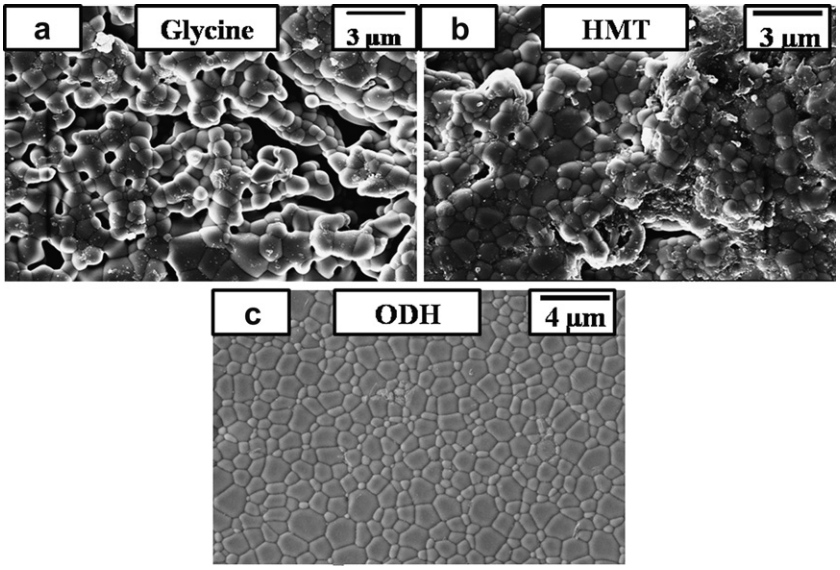

Fig. 3. FESEM images of GDC pellets (sintered at 1300 °C/5 h) prepared from powders synthesized using different fuels.

In an effort to study the influence of sintering strategies and sintering methodologies on the final microstructure and effectiveness of methods in retaining the sub-micron sized crystallites, we adopted conventional ramp and hold sintering (CRHS), microwave sintering (MWS) and two-stage sintering (TSS). MWS is a well known technique that exploits the heat generated within the material owing to the ability of the material to couple with the microwave. Recently explored TSS methodology utilizes the principle that the activation energy for grain growth is lower than the activation energy of densification [25]. The suppression of the final-stage grain growth is achieved by exploiting the difference in kinetics between grain-boundary diffusion and grain-boundary migration. The sintering schedule is characterized by two regimes wherein the first regime at peak temperature dominates densification and complete elimination of residual porosity followed by a second regime at significantly lower temperatures effecting controlled grain growth during final stages of sintering. Sintering schedule employed in three different methods in the present investigation is summarized in Fig. 4. Both the methods resulted in a dense microstructure with density levels >97%. Fig. 5 depicts the microstructure of the polished and thermally etched samples fabricated from these two methods. While MWS resulted in slight reduction in the overall grain size (Fig. 5b), two-stage sintering curtailed the grain growth substantially (∼500 nm) (Fig. 5a). However, the grain size was larger than expected. Further reduction in grain size can be expected on fine tuning the sintering schedule based on the detailed dilatometric studies.

Complex impedance analysis was performed to calculate the overall conductivity and to separate the contributions from different electro-active components of the ceramics, namely, grain, grain boundary and electrode/sample interface. Inset (1) of Fig. 6 depicts the impedance spectra that are expected from ion-conducting ceramics. In the impedance response, high-frequency semicircle is ascribed to the grain contribution, intermediate semicircle originates from the grain boundary and the low frequency arc is associated with the electrode–sample interface. Contribution from each component could be modeled using a parallel RC (Resistor and Capacitor) circuit or *R* (CPE) (resistor and constant phase element) circuit. A Z* plot for GDC–ODH ceramics at 400 °C (Fig. 6) contains a large arc with non-zero intercept at high frequencies and an arc at low frequency. The high-frequency non-zero intercept, which evolves into semicircle at low temperatures

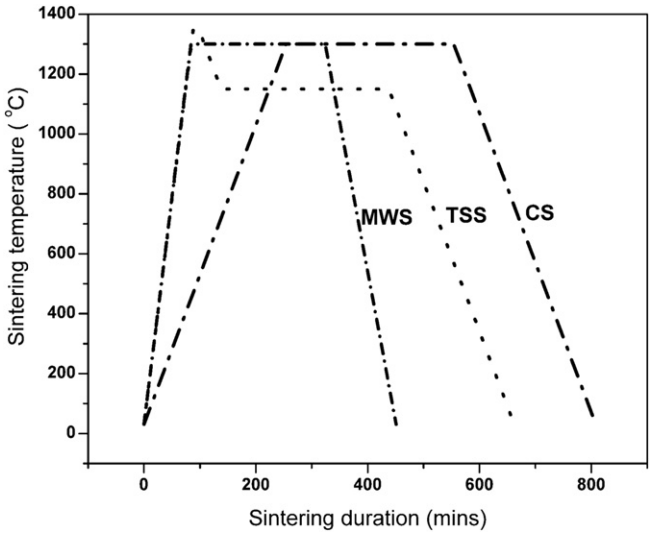

Fig. 4. Sintering schedule employed in conventional ramp and hold sintering, microwave sintering and two-stage sintering.

(Inset 2 of Fig. 6) corresponds to the grain bulk resistance (R_b) and the depressed semicircle in the middle-frequency region represents the grain boundary (R_{gb}) response. Arc at the low-frequency region may be attributed to electrode resistance (R_{elect}). It can be seen that the grain boundary conductivity is lower than the bulk conductivity by at least one order of magnitude. Nonetheless, grain boundary semicircle diameter reduces with increasing temperature and semicircle is barely visible at 600 °C indicating that the contribution of grain-boundary resistance to the present electrolyte powder synthesized through combustion reaction (GDC–ODH) at the operating temperature of the IT-SOFC is low. Low grain boundary resistance could be due to the dense microstructure of the GDC–ODH samples, as presence of porosity generally contributes to the grain boundary resistance of the samples. Samples from other GDC powders exhibited a substantial grain boundary contribution at 600 °C owing to the porous nature of the samples. Fig. 7 presents the Arrhenius plots of the bulk, grain boundary and total conductivities of the GDC–ODH samples fired at 1300 °C/5 h. Electrical conductivities of the bulk, grain boundary and the total conductivities of GDC–ODH samples at 400 °C along with the activation energies are provided in Fig. 7. Total conductivity values and total activation energy are very near to those corresponding to the grain boundary conductivity, indicating that the rate-limiting step for conductivity is the grain boundary one. However, tendency of grain and the grain boundary Arrhenius plots to approach each other with increase in temperature clearly suggests that grain boundary barrier decreases with increase in temperature. Table 3 summarizes the conductivity values obtained for the GDC–ODH samples at 400 °C along with the conductivities of GDC–HMT, GDC–glycine samples. Conductivity values of GDC–HMT and GDC–glycine samples are much lower than that of GDC–ODH samples, probably due to the porosities in the samples. Presence of pores is detrimental to the ionic conduction due to the "blocking effect".

Reported conductivity values of GDC in the literature vary between 7.6×10^{-4} to 2.7×10^{-3} Scm^{-1} at 400 °C [4,5,13,26–30]. Since sintering temperature, density, grain size in different samples is different, comparing their conductivity values and claiming the superiority of one over other, is inappropriate. High electrical conductivity values (∼1.9×10^{-4} Scm^{-1} at 400 °C) have been reported for the low-temperature sintered (∼1000 °C), fine grain sized (∼200 nm) GDC electrolyte samples prepared from weakly-agglomerated powders synthesized by homogeneous precipitation process [31]. In these samples level of agglomeration is reported to be very low. High electrical conductivity (∼1.7×10^{-3} Scm^{-1} at 400 °C) has also been reported for sintering aid assisted, low temperature sintered, GDC samples [28,29].Though electrical conductivity of the present sample is in par or better than the most of the reported values, their values are lower than the fine grain sized samples. Even sub-micron sized (∼400 nm) TSS samples did not show significant improvement in the conductivity. Improved conductivity was not observed in GDC–ODH prepared in the present study as the grain size in the samples was higher than the threshold value (∼100 nm). We believe that nano GDC–ODH powders have the necessary characteristics to result in nanosized grains on sintering on further fine tuning of the TSS sintering strategy.

As GDC–ODH powders exhibited the necessary powder and electrical characteristics, they were further probed to evaluate their suitability for WPS. The spray-coating process involves several important steps: preparation of stable suspension, spray-coating of suspension, drying of wet coating, and sintering. Among these steps, formation of a stable suspension is critical and prerequisite to obtain dense coatings for WPS. Suitability of the GDC powders under study for WPS was investigated by preparing the suspension. GDC–ODH and GDC–glycine powders were ball milled for 10 h in

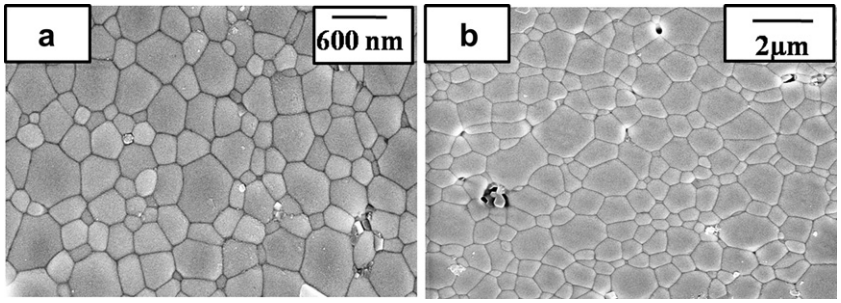

Fig. 5. FESEM images of GDC pellets fabricated by (a) Two-stage and (b) microwave sintering.

isopropyl alcohol. The solid content of the suspension was 5 mass %. In order to obtain a well-dispersed suspension, nonionic surfactant Triton X-100 was added as a dispersant. Fig. 8 shows the GDC–ODH and GDC–glycine suspensions aged at room temperature for few hours. After aging, the GDC–ODH suspension did not display any sedimentation, while the GDC–glycine particles separated from the liquid. Stability of the GDC–glycine samples did not improve on further increasing the amount of Triton-X. The high stability of the GDC–ODH colloidal suspension can be attributed to its fine particle size, which resisted sedimentation by Brownian motion. Because of the higher degree of agglomeration in GDC–glycine brownian forces were not strong enough to overcome the gravitational force and hence resulted in sedimentation. Unstable suspensions generally result in coatings with high porosity levels. Formation of stable suspension and ability for low temperature sintering on conventional pressing and sintering suggests that GDC–ODH powders have necessary characteristics for WPS. WPS of GDC–ODH suspension is in progress.

Among all the powders, GDC–glycine + AA powders exhibited necessary size requirements, shapes (blocky angular) and flowability values (100 s/50 g) suitable for efficient APS. In plasma sprayed coatings, characteristics such as splat density, inter splat adhesion are strongly influenced by the stock powder characteristics such as particle size, shape, flowability, specific mass, etc. Challenge in APS is to develop dense, pore free, gas tight electrolytes as plasma spraying generally leads to coatings with poor inter splat adhesion, inter splat cracks and inter-granular pores which lead to the diffusion of fuel or air through the electrolyte [20,32]. In the present study, as specific mass of GDC–glycine + AA is low, spraying parameter such as feed rate, power conditions, etc., had to be optimized to achieve substantial thickness during the deposition. Fig. 9 shows the cross-sectional microstructure of plasma sprayed coatings fabricated from GDC–glycine + AA powders. Features of these coatings are very different from the ones that we observed in plasma sprayed coatings of YSZ fabricated using stock powders prepared by spray drying and the ones reported in the literature [33,34]. Cross-sectional microstructures of plasma sprayed coatings are generally characterized by distinctive lamellar microstructure with a columnar grain structure in a direction perpendicular to the lamellae. On the contrary, present coatings appeared to possess good inter splat adhesion and free from the features mentioned above.

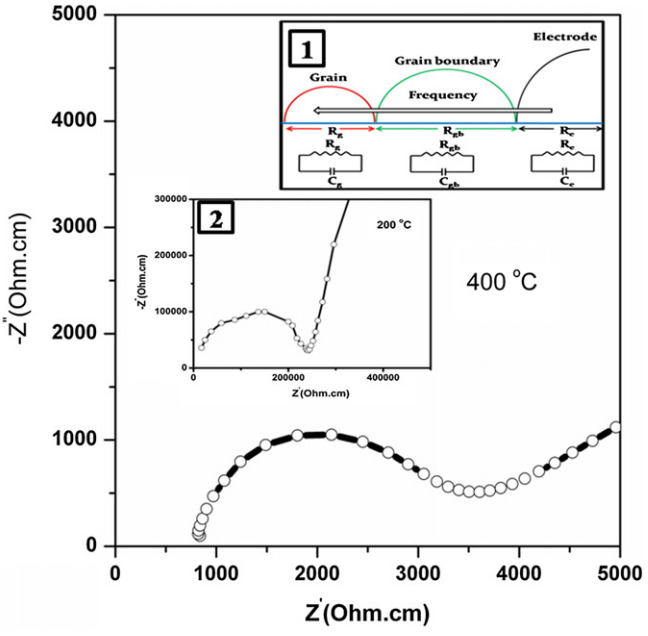

Fig. 6. Impedance plot for GDC ceramics at 400 °C. Inset (1) - impedance spectra that are expected from an ion-conducting ceramic, Inset (2)- impedance plot for GDC at 400 °C.

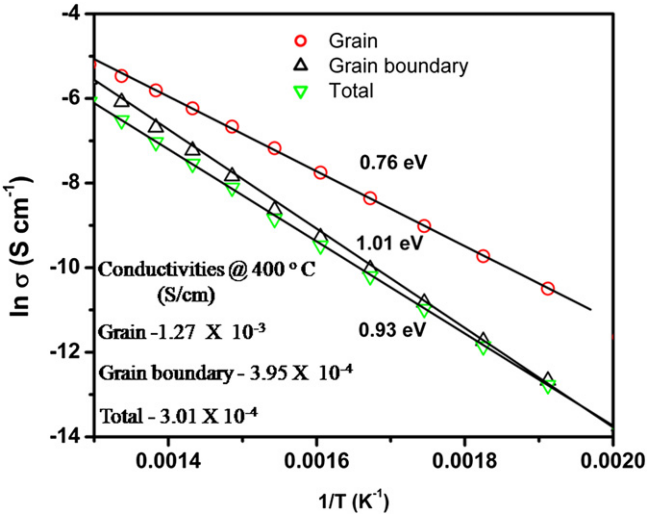

Fig. 7. Arrhenius plots of the bulk, grain boundary and total conductivities of GDC pellets.

Table 3
Electrical conductivities of GDC–ODH, GDC–HMT, GDC–glycine samples sintered at 1300 °C/5 h.

Sample	σ @ 400 °C (Scm^{-1})
GDC–ODH	3.01×10^{-4}
GDC–HMT	1.3×10^{-4}
GDC–glycine	8.1×10^{-5}

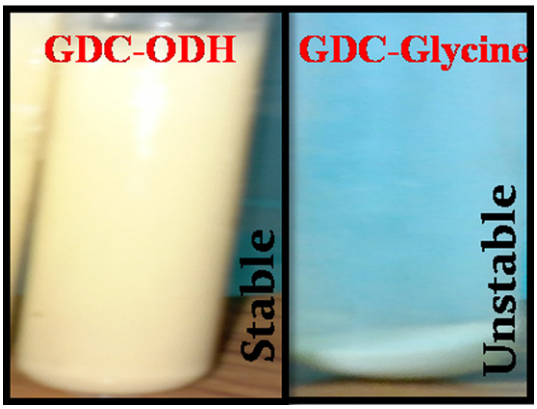

Fig. 8. GDC–ODH and GDC–glycine suspensions aged at room temperature for few hours.

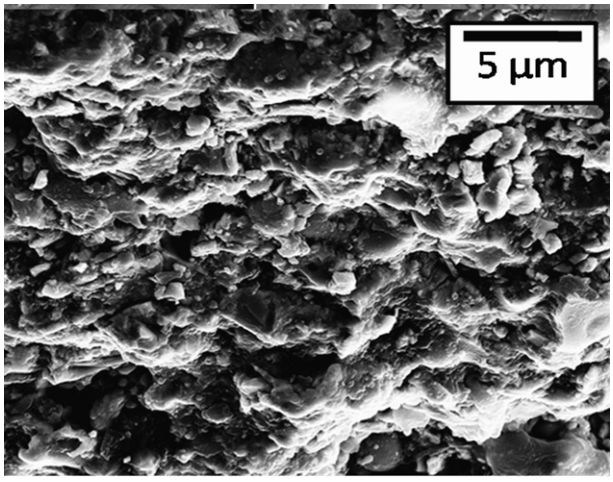

Fig. 9. Cross-sectional microstructure of plasma sprayed coating fabricated from GDC–Glycine + ammonium acetate powder.

During plasma spraying, essential criteria to obtain dense coating is the complete melting of stock powder particles in plasma. Melting level of the particle depends on the effectiveness of heat transfer from the plasma to and through the particle. Effective heat transfer to SCS derived powder can be attributed to the combined heat flow assisted by both conduction and convection. Porous microstructure results in the effective heat transfer and complete melting of the particles. Attaining such a dense coating in APS is essential not only to prevent gas leak, but also to achieve good ionic conductivity. Ionic conductivity of plasma sprayed coatings are generally about 1/10th to 1/3rd of the bulk samples due to the poor inter splat adhesion [34–37]. APS coatings from combustion powders are expected to have high conductivity due to good inter splat adhesion. Attempts are under progress to obtain free forms of GDC by APS to perform conductivity measurements.

4. Conclusions

Solution combustion synthesis was employed to synthesize GDC powders of varying powder characteristics by using different fuels. Nano particle sized GDC powder prepared by using oxalylyl dihydrazide fuel exhibited higher sinteractivity and resulted dense pellet with high conductivity (3×10^{-4} Scm^{-1} at 400 °C). These powders exhibited necessary characteristics suitable for wet powder spraying. Due to the high reaction temperature agglomerated particles were formed on using glycine as fuel. Use of ammonium acetate fuel along with reduced amount of glycine yielded micron sized, plasma sprayable grade GDC powder. These powders resulted in a dense atmosphere plasma sprayed coating with superior inter splat adhesion. Present study demonstrates that simple, cost effective, single step solution combustion method has the versatility to produce powders of varying characteristics suitable for various fabrication techniques of SOFC electrolyte. Overall cost reduction in the fabrication of SOFC can be achieved by employing solution combustion method for the synthesis of powders required for fabricating different components of solid oxide fuel cells.

Acknowledgments

The authors acknowledge CSIR, SIP-SED-06 for funding the project and the director, NAL-CSIR, for the encouragement. The authors are thankful to Mr. N. Balaji for APS of coatings and Mr. Siju for SEM studies. Help received from Miss. Neha Singh in the impedance measurement is also highly appreciated.

References

[1] D.J.L. Brett, A. Atkinson, N.P. Brandon, S.J. Skinner, Chem. Soc. Rev. 37 (2008) 1568–1578.
[2] S. Hui, J. Roller, S. Yick, X. Zhang, C. Decès-Petit, Y. Xie, R. Maric, D. Ghosh, J. Power Sources 172 (2007) 493–502.
[3] H. Inaba, H. Tagawa, Solid State Ionics 83 (1996) 1–16.
[4] B.C.H. Steele, Solid State Ionics 129 (2000) 95–110.
[5] Z. Tianshu, P. Hing, H. Huang, J. Kilner, Solid State Ionics 148 (2002) 567–573.
[6] N.H. Menzler, F. Tietz, S. Uhlenbruck, H.P. Buchkremer, D. Stöver, J. Mater. Sci. 45 (2010) 3109–3135.
[7] A.J. Jacobson, Chem. Mater. 22 (2010) 660–674.
[8] B. Djuričić, S. Pickering, J. Eur. Ceram. Soc. 19 (1999) 1925–1934.
[9] Y.B. Go, A.J. Jacobson, Chem. Mater. 19 (2007) 4702–4709.
[10] J.G. Li, T. Ikegami, T. Mori, Acta Mater. 52 (2004) 2221–2228.
[11] S. Nakane, T. Tachi, M. Yoshinaka, K. Hirota, O. Yamaguchi, J. Am. Ceram. Soc. 80 (1997) 3221–3224.
[12] A.I.Y. Tok, L.H. Luo, F.Y.C. Boey, Mater. Sci. Eng. A 383 (2004) 229–234.
[13] T.S. Zhang, J. Ma, L.H. Luo, S.H. Chan, J. Alloys Compd 422 (2006) 46–52.
[14] S.T. Aruna, A.S. Mukasyan, Curr. Opin. Solid State Mater. Sci. 12 (2008) 44–50.
[15] K.C. Patil, S.T. Aruna, S. Ekambaram, Curr. Opin. Solid State Mater. Sci. 2 (1997) 158–165.
[16] K.C. Patil, S.T. Aruna, T. Mimani, Curr. Opin. Solid State Mater. Sci. 6 (2002) 507–512.
[17] M.S. Kaliszewski, A.H. Heuer, J. Am. Ceram. Soc. 73 (1990) 1504–1509.
[18] J.G. Li, T. Ikegami, J.H. Lee, T. Mori, Acta Mater. 49 (2001) 419–426.
[19] H. Shi, W. Zhou, R. Ran, Z. Shao, J. Power Sources 195 (2010) 393–401.
[20] C.J. Li, C.X. Li, X.J. Ning, Vacuum 73 (2004) 699–703.
[21] C.J. Li, X.J. Ning, C.X. Li, Surf. Coat. Technol. 190 (2005) 60–64.
[22] D. Stöver, D. Hathiramani, R. Vaßen, R.J. Damani, Surf. Coat. Technol. 201 (2006) 2002–2005.
[23] P. Fauchais, J. Phys. D: Appl. Phys. 37 (2004) R86–R108.
[24] R. Hui, Z. Wang, O. Kesler, L. Rose, J. Jankovic, S. Yick, R. Maric, D. Ghosh, J. Power Sources 170 (2007) 308–323.
[25] P.C. Yu, Q.F. Li, J.Y.H. Fuh, T. Li, L. Lu, J. Mater. Process. Technol. 192-193 (2007) 312–318.
[26] S. Zha, C. Xia, G. Meng, J. Power Sources 115 (2003) 44–48.
[27] S.H. Jo, P. Muralidharan, D.K. Kim, Solid State Ionics 178 (2008) 1990–1997.
[28] C. Kleinlogel, L.J. Gauckler, Solid State Ionics 135 (2000) 567–573.
[29] V. Gil, J. Tartaj, C. Moure, P. Durán, J. Eur. Ceram. Soc. 26 (2006) 3161–3171.
[30] K. Huang, M. Feng, J.B. Goodenough, J. Am. Ceram. Soc. 81 (1998) 357–362.
[31] P. Muralidharan, S.H. Jo, D.K. Kim, J. Am. Ceram. Soc. 91 (2008) 3267–3274.
[32] J. Ilavsky, C.C. Berndt, J. Karthikeyan, J. Mater. Sci. 32 (1997) 3925–3932.
[33] Y.Z. Xing, C.X. Li, C.J. Li, H.G. Long, Y.X. Xie, Solid State Ionics 179 (2008) 1483–1485.
[34] Y.Z. Xing, C.J. Li, Q. Zhang, C.X. Li, G.J. Yang, J. Am. Ceram. Soc. 91 (2008) 3931–3936.
[35] C.J. Li, C.X. Li, Y.Z. Xing, M. Gao, G.J. Yang, Solid State Ionics 177 (2006) 2065–2069.
[36] C.J. Li, A. Ohmori, J. Therm. Spray Technol. 11 (2002) 365–374.
[37] Y.Z. Xing, C.J. Li, C.X. Li, G.J. Yang, J. Power Sources 176 (2008) 31–38.